MRS Communications (2014), *4*, 7–13
© Materials Research Society, 2014
doi:10.1557/mrc.2014.4

MRS Communications

Research Letters

Oxygen vacancy enhanced room-temperature ferromagnetism in Sr_3SnO/c-YSZ/Si (001) heterostructures

Y.F. Lee, F. Wu, J. Narayan, and **J. Schwartz,** Department of Materials Science and Engineering, North Carolina State University, Raleigh, North Carolina 27695-7907

Address all correspondence to Yi-Fang Lee at **ylee9@ncsu.edu**

(Received 22 October 2013; accepted 6 January 2014)

Abstract

The magnetic properties of Sr_3SnO (SSO) epitaxial thin films prepared under various post-growth annealing treatments are reported. The SSO films are grown on cubic yttria-stabilized zirconia Si (001) platform by pulsed laser deposition. Post-growth vacuum annealing is found to enhance the room-temperature ferromagnetism (RTFM), whereas oxygen annealing reduces it. The results are explained through the oxygen vacancy constituted bound magnetic polarons (BMP) model. An empirical relationship between the extracted BMP concentration and the oxygen vacancy concentration is shown using X-ray photoelectron spectroscopy data. The results indicate a promising way to tune RTFM by manipulating oxygen vacancies and related defects.

Topological insulators (TIs) are an emerging class of materials that have generated great interest because of their unique properties that may enable their use in quantum computing and spintronics.[1,2] The discovered TIs in three dimensions (3D) are non-magnetic insulators with time-reversal symmetry (TRS) protected by gapless surface states.[3] It is important to break the TRS of TIs by combining external perpendicular ferromagnetic coupling envisaged for practical applications.[4] A natural strategy to achieve this is through doping of transition metal (TM) elements with spin orientation out of the surface plane, as demonstrated by the success of dilute magnetic semiconductors (DMSs).[5]

Introducing magnetic ions into TI materials is an effective way to generate robust magnetism and open a surface energy gap resulting in the emergence of massive Dirac fermions. Furthermore, precise, simultaneous control of magnetic, and charge doping can alter the Fermi-energy (E_F) level inside the Dirac gap.[6,7] By using TM elements, such as Cr and Fe, the 3D TIs Bi_2Te_3, Bi_2Se_3, and Sb_2Te_3 have become magnetically ordered insulators. The ferromagnetic moments resulting from TM-doped TI systems has been theoretically proposed through the van Vleck mechanism and the Ruderman–Kittel–Kasuya–Yosida mechanism.[8] Based on these peculiar properties and interesting phenomenon, the intricate interplay between topological order and ferromagnetism (FM) is expected to give rise to a variety of unconventional effects that may lead to new device paradigms.[6,9]

Recently, many undoped oxides, such as ZnO, TiO_2, In_2O_3, SnO_2, and HfO_2, have been reported to show FM features, although the origin of such FM is not well understood.[10,11] The most plausible origin of such FM properties in otherwise non-magnetic oxides is defects, such as strain and non-equilibrium point defects inferred to be oxygen vacancies, cation vacancies, and interstitials, which result directly from processing.[12–14] In TiO_2 and HfO_2, FM has been attributed to the presence of oxygen vacancies, which are presumed to behave as an n-type dopant, and the existing vacancies tailor the physical properties of the films.[15,16] In ZnO, room-temperature ferromagnetism (RTFM) arises from unpaired electrons of oxygen atoms around the Zn vacancies, whereas carrier concentrations are derived from oxygen vacancies and Zn interstitial complexes.[17]

Sr_3SnO (SSO) has been identified theoretically by Klintenberg as a potential TI material with the required band-inversion at the Γ-point in the presence of spin orbital coupling (SOC).[18] SSO has an inverse perovskite structure and crystallizes in the cubic system with space group *Pm3m* and a theoretical unit cell of 0.512 nm. Throughout the Brillouin zone it has an indirect local density approximation (LDA) band gap of 0.1 eV.[18,19] Recently, we reported that, even in the absence of TM ions, single-crystal SSO thin films are DMSs with RTFM.[20] In the current work, we unravel the origin of RTFM in SSO and show a clear relationship between RTFM and oxygen vacancies. In particular, we find that post-growth vacuum annealing (VA) enhances the RTFM, whereas oxygen annealing (OA) degrades it.

The primary focus of this study is to elucidate the origin of RTFM in epitaxial SSO single-crystal thin films through measurements of the impact of different post-growth annealing treatments on magnetic properties. X-ray photoelectron

https://doi.org/10.1557/mrc.2014.4 Published online by Cambridge University Press

spectroscopy (XPS) and superconducting quantum interference device (SQUID) magnetization data indicate that the intrinsic point defects associated with oxygen vacancies are the most promising candidates to manifest RTFM in this system. As a consequence, it is postulated that large concentrations of intrinsic defects form an impurity band that is the source of d^0 magnetism. The observed RTFM in SSO thin films is interpreted in terms of a bound magnetic polaron (BMP) model, where an impurity band resulting from oxygen vacancies locally trap electrons that occupy an orbital overlapping the surrounding magnetic moments.

The SSO/c-YSZ/Si (001) thin-film heterostructures are grown by sequentially ablating c-YSZ, SrO, and SnO_2 targets using an LPX 100 KrF pulsed excimer. The SSO films require alternating laser pulses; here a 5:1 ratio of SrO:SnO_2 pulses are used at 750 °C under 5×10^{-3} torr oxygen pressure. The films are then annealed within the PLD chamber at 750 °C under 1×10^{-1} torr oxygen pressure for 3 h. More details regarding sample preparation are found in.[20]

The structure of the SSO films is characterized by x-ray diffraction (XRD) $\theta - 2\theta$ scans using a Rigaku x-ray diffractometer with Cu K_α radiation ($\lambda = 0.15418$ nm). Microstructural analysis is performed using a JEOL-2010 field-emission high-resolution transmission electron microscope (HRTEM). XPS is performed on a SPECS FlexMod equipped with an Al K_α monochromatic x-ray source (1486.7 eV) to clarify contamination concerns, characterize the surface state, and estimate the oxygen vacancy content within the SSO thin films. The magnetic properties of three SSO films: one as-grown (pristine), one OA post-growth, and one VA post-growth, are measured using a Quantum Design SQUID magnetometer. OA is performed at 750 °C under full oxygen ambient (~760 torr) for 3 h, whereas VA is performed at 750 °C for 3 h at 5×10^{-6} torr. For the zero-field cooled (ZFC) magnetic data, the sample is cooled to 5 K in the absence of magnetic field and the magnetization is measured while warming to 400 K in the presence of a 100 Oe magnetic field. The field cooled (FC) data are taken while warming the sample after cooling to 5 K in the presence of a 100 Oe field. Magnetization hysteresis is measured by sweeping the magnetic field from −1 to +1 T at 300 K.

The oxygen partial pressure during deposition plays a key role as an oxidizing agent to help form and stabilize the desired crystalline phase at the deposition temperature. Figure 1(a) displays the $\theta - 2\theta$ XRD pattern of the SSO/c-YSZ/Si (001) heterostructure collected after varying the oxygen partial pressure for a 5:1 SrO:SnO_2 pulse ratio. As the oxygen partial pressure increases, the Sr_2SnO_4 (200) peak decreases. For an oxygen partial pressure of 5×10^{-3} torr, only the SSO phase is found and no additional peaks are observed. Both c-YSZ and SSO exhibit [001] preferred orientation single crystallographic peaks, suggesting that films are highly textured or epitaxial. Note that no additional peaks are observed for OA, pristine or VA samples, excluding the possibility of formation of any other phase [Supplementary material I (a)]. High-resolution XRD shows that, for the VA sample, the c-YSZ (002), and SSO (002) peaks shift from $2\theta = 34.82°$ (c-YSZ_{bulk}) and $2\theta = 34.88°$ (SSO_{bulk}) and that there is a large increase in the full width at half maximum (FWHM). These results indicate an increase in the concentration of intrinsic point defects and oxygen vacancies [Supplementary material I (b)].

The TEM study reveals the microstructure and verifies the epitaxial relationship of the films. HRTEM <110> cross-sectional images of epitaxial c-YSZ/Si and SSO/c-YSZ interfaces are shown in Figs. 1(b) and 1(c) along with their fast Fourier transform (FFT) diffraction patterns. The highly epitaxial growth of the c-YSZ film on Si is evident in the HRTEM image. The existence of amorphous SiO_x does not alter the epitaxial growth of the buffer layer, because the epitaxial buffer layer has been formed before the SiO_x. The sharp and smooth SSO/c-YSZ interface, with no indication of an interfacial layer, is also seen. No misfit dislocations at the coherent interface between SSO and c-YSZ are identified owing to very small in-plane lattice mismatch (0.311%) and low interfacial energy. Even after several hundred atomic layers of coherent epilayer growth, the strain energy is insufficient to overcome the activation energy for dislocation nucleation at the free surface. The selected area electron diffraction (SAED) pattern (not shown) confirms the epitaxial nature of the layers with cube-on-cube orientation relationship: (001)[100]SSO||(001)[100]c-YSZ||(001)[100]Si.

The in-plane magnetization hysteresis curves at 300 K for the three different sample types are shown in Fig. 2(a). The diamagnetic contribution from the substrate and paramagnetic contribution from the c-YSZ buffer layer have been subtracted. For each sample condition (OA, pristine, and VA), a sample without the SSO layer was prepared and characterized so the respective contributions can be subtracted accurately. Clear saturation and hysteretic behaviors are observed, providing evidence of FM behavior at 300 K. The VA and OA samples show the largest and smallest saturation moments (M_s), respectively. The top left inset compares the coercivities (H_c) and M_s for each sample, indicating that there is a significant enhancement in FM after VA. The bottom right inset shows the low-field portion of the magnetization hysteresis loops to delineate the FM behavior up to 300 K. During VA, oxygen vacancies migrate and form clusters to reduce the system energy, favoring a decrease in the strain-free energy.[21] Banerjee et al. demonstrated that the large moments can be generated owing to oxygen vacancy clusters in undoped ZnO.[22] Coey et al. further proposed that oxygen vacancies can cause a change of band structure in the host oxides and contribute significantly to the FM.[23] According to the results shown here, the oxygen vacancies play a crucial role in tailoring the RTFM within the SSO system as well.

The temperature dependence of the magnetization has been studied through FC and ZFC measurements from 5 to 400 K; results are plotted in Fig. 2(b). By taking the difference between these two quantities, $\Delta M = M_{FC} - M_{ZFC}$, the para- and diamagnetic contributions to the magnetization are subtracted, leaving

https://doi.org/10.1557/mrc.2014.4 Published online by Cambridge University Press

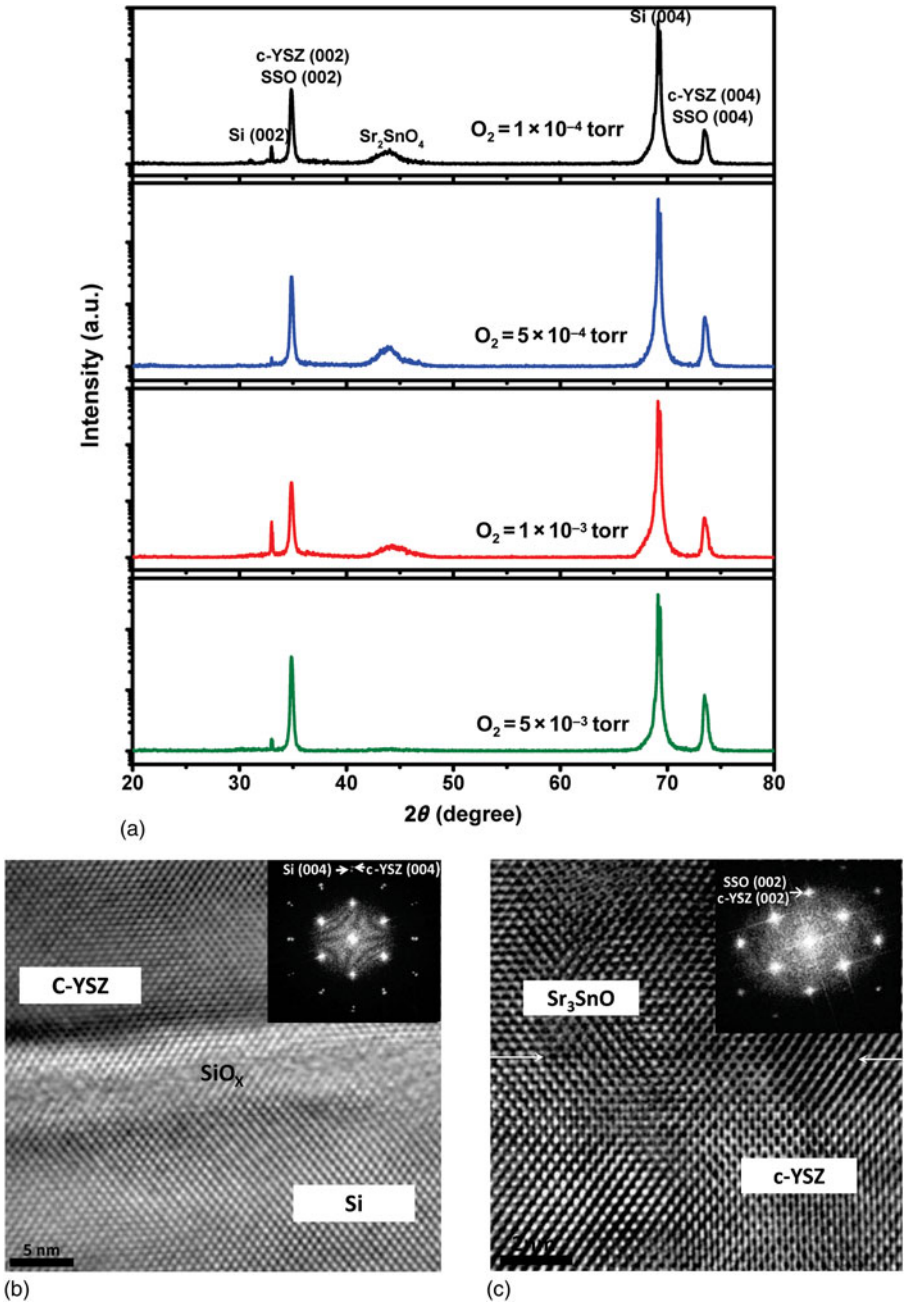


Figure 1. (a) XRD pattern of SSO/c-YSZ/Si(100) heterostructures under different oxygen partial pressures; and high-resolution TEM [110] cross-sectional images at the interface of (b) epitaxial c-YSZ/Si, and (c) epitaxial SSO/c-YSZ. The insets show the FFT patterns.

only a measure of the hysteretic FM regime. The Curie temperature (T_C) of all samples is above 300 K. The pristine and VA samples display non-zero magnetization up to 400 K, implying a robust FM signature. The OA sample shows nearly zero magnetization at ~320 K. Thus, the thermoremanent magnetization (ΔM) has been enhanced significantly by VA as compared to OA in the entire temperature range. For the VA sample, which has the largest H_c and M_s, the separation between the FC and ZFC data exists at a higher temperature, as seen in Fig. 2(b) inset. This is consistent with the presence of FM ordering and suggests that the enhanced FM upon VA is directly related to the creation of additional oxygen vacancies. The quantification of oxygen vacancies as analyzed by XPS O1s spectra is discussed below.

Several mechanisms have been proposed to explain the origin of FM in DMSs. In addition to the magnetic doping effect, oxygen vacancies have been suggested as the origin of the magnetic behavior.[24] An oxygen vacancy can catch an itinerant

https://doi.org/10.1557/mrc.2014.4 Published online by Cambridge University Press

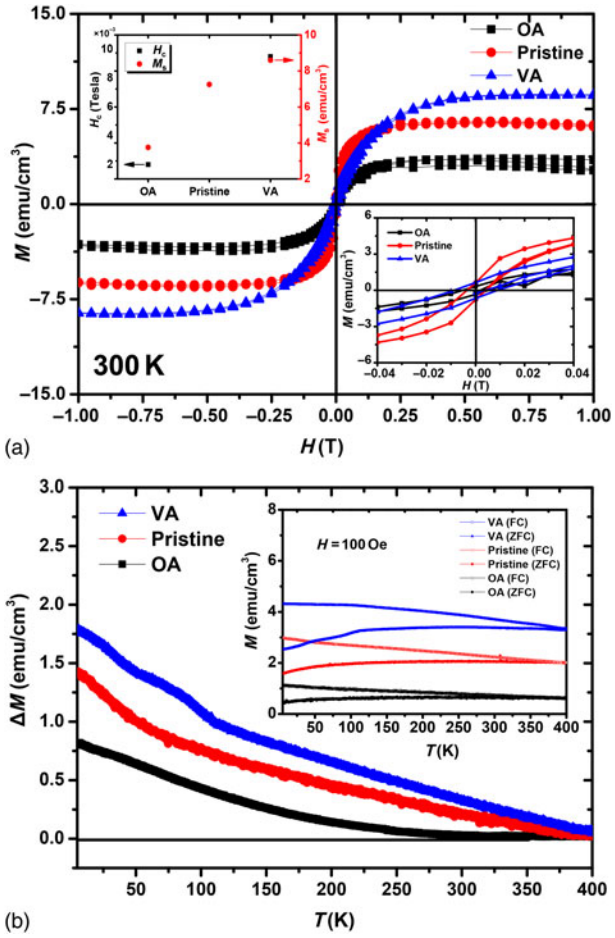


Figure 2. (a) Room-temperature magnetization hysteresis of pure SSO films under different post-growth annealing treatments. Inset (top left) compares of H_c and M_s under different treatments. Inset (right bottom) is the enlarged $M-H$ loops for -0.04 to $+0.04$ T, showing the hysteresis and coercivity more clearly. (b) Temperature dependence of the difference in magnetization between FC and ZFC for oxygen-annealed, pristine, and vacuum-annealed samples. The inset is the temperature dependence of the magnetization under a 100-Oe applied field.

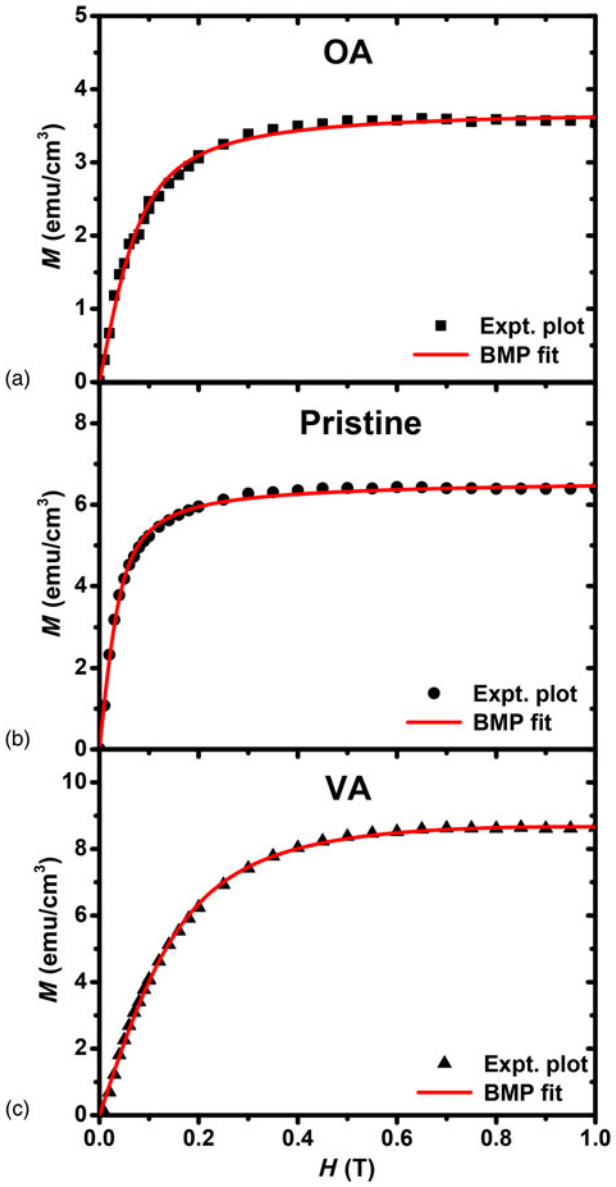


Figure 3. Initial portion of the $M-H$ curve fitted with the BMP model [Eq. (1)] for (a) oxygen-annealed, (b) pristine, and (c) vacuum-annealed samples. The symbols are the experimental data and the solid lines are the fit using the BMP model. Extracted parameters are shown in Table I.

electron to form a "hydrogen-like" orbit[25] with a finite radius and become a distorted oxygen vacancy O^+ site in the absence of applied electric field or doping. A polaron is a quasiparticle formed by a charged particle, such as an oxygen vacancy defect, and the resulting lattice polarization phonon field. The results here indicate that the oxygen vacancy constituted BMP model is a promising candidate for explaining the origin of RTFM in SSO. A clear magnetization hysteresis loop, with enhanced M_s and H_c, is observed in the VA sample due to the increased concentration of oxygen vacancies. In the BMP model, oxygen vacancies are responsible for the shallow donors and strongly stabilize the ferromagnetic ground state.[25] An electron associated with a donor defect, such as an oxygen vacancy, is confined in a hydrogenic orbit. As more oxygen vacancies are produced during VA, more electrons become bound to the oxygen vacancies. To maintain the local charge balance and stabilize the structure, other point defects such as cation interstitials or vacancies, are generated. As a result, the greater density of oxygen vacancies leads to more interactions with the host lattice environment for charge redistribution and produces more overlapping BMPs and more percolation, thereby enhancing the FM strength.[26]

To better determine the suitability of the BMP model to the observed data, the M versus H data were fit to the BMP model following Chiorescu et al.[27]. According to the BMP model, the measured magnetization

$$M = M_0 L(\chi) + \chi_m H, \quad (1)$$

https://doi.org/10.1557/mrc.2014.4 Published online by Cambridge University Press

Table I. Fitting parameters extracted from the BMP model at 300 K.

	M_0 (emu/cm^3)	m_{eff} (emu)	χ_m	N (cm^{-3})
Oxygen annealed	3.79	2.07×10^{-19}	7.73×10^{-6}	1.83×10^{19}
Pristine	6.54	2.98×10^{-19}	6.88×10^{-6}	2.19×10^{19}
Vacuum annealed	8.86	3.36×10^{-19}	4.27×10^{-6}	2.64×10^{19}

where the first term on the right-hand side is the BMP contribution and the second term is the paramagnetic matrix contribution. Here, $M_0 = Nm_s$, where N is the number of BMPs involved and m_s is the effective spontaneous moment per BMP. $L(\chi) = \coth(\chi) - 1/\chi$ is the Langevin function with $\chi = m_{eff}H/(k_BT)$, where m_{eff} is the true spontaneous moment per BMP which, at higher temperature, can be approximated as $m_s = m_{eff}$. Thus, for a good approximation, the $M - H$ data can be analyzed in terms of Eq. (1), with M_0, m_{eff}, and χ_m used as fitting parameters. The experimental data along with fitted data are shown in Figs. 3(a)–3(c) for the OA, pristine, and VA samples, respectively, at 300 K. The resulting fitted curves closely follow the experimental data and the extracted parameters are tabulated in Table I. The total BMP magnetization M_0 values are found to be of the order of 3–8 emu/cm^3. For the VA sample, M_0 is found to be the highest; this is due to higher oxygen vacancy concentration. The spontaneous moment per BMP, m_{eff}, is found to be of the order of 10^{-19} emu. Assuming $m_s = m_{eff}$, the BMP concentration is estimated to be of the order of 10^{19} cm^{-3}. The BMP concentration follows the trend of VA > pristine > OA, in accordance with M_0 values. The values are reasonable as compared to the required concentration of BMPs in order to percolate through a ZnO lattice ($\sim 10^{20}$ cm^{-3}).[28] The temperature-dependent electrical resistivities for temperature ranging from 50 to 300 K are provided as a Supplementary material II (a); the resistivities and carrier concentrations at 300 K are found in Supplementary material II (b). Thermal annealing in oxygen leads to oxygen diffusion into the film and a reduction in the oxygen vacancy concentration. Thus, the resistivity increases significantly relative to the VA sample and the carrier concentration decreases from $\sim 10^{19}$ cm^{-3} to $\sim 10^{18}$ cm^{-3}.

The oxygen vacancy concentrations are quantified using XPS spectra. The XPS survey spectra of the pristine sample is shown in Fig. 4(a), indicating that Sr, Sn, and O are the only elements observed, except for a small amount of environmental C; no additional peaks are detected. All peaks reported are charge corrected using the C 1s peak position at 284.5 eV as a reference point. Figure 4(b) shows the high-resolution O 1s XPS spectra of VA and OA samples. In both cases, the O 1s peak shows broad, asymmetric peaks that are fitted with two Gaussian peaks, indicative of two different oxygen contributions. The main emission peak (O_{II}) is detected at ~529.4 eV and the accompanied smaller shoulder peak (O_I) is at ~531.4 eV. The first peak is commonly ascribed to lattice oxygen,[29] whereas Chuang et al.[30] found that the peak around 530.7–531.6 eV is caused by oxygen inside a non-stoichiometric oxide within the surface region of the material; these are oxygen vacancies. Although it is not possible to

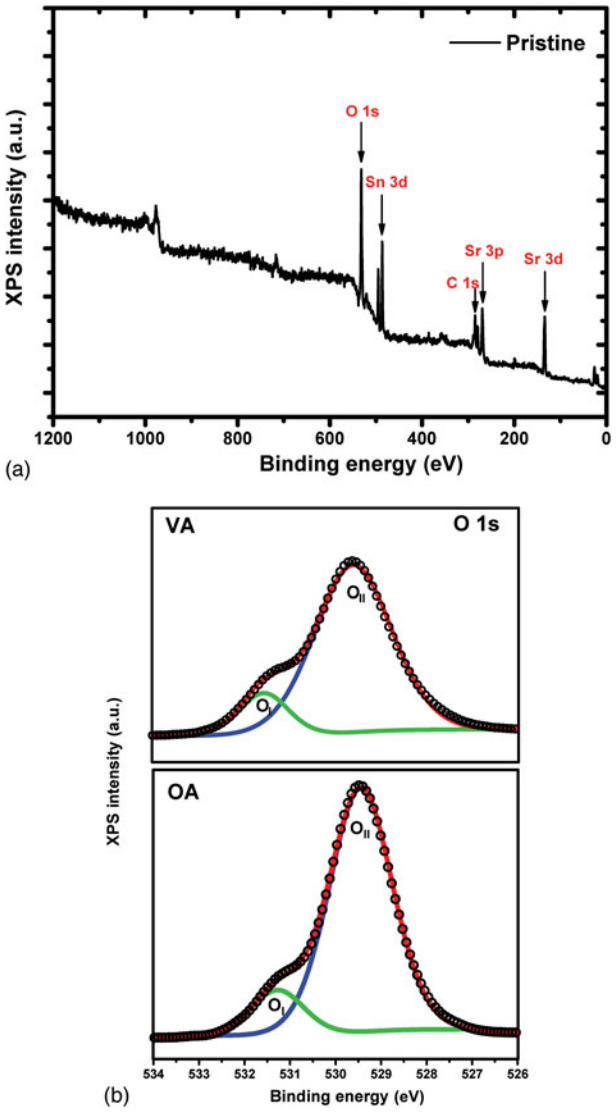


Figure 4. (a) XPS survey spectra of a pristine SSO thin film and (b) XPS high-resolution scan of the oxygen 1s peak for vacuum-annealed and oxygen-annealed SSO films. The O 1s spectra are decomposed into a main peak (O_{II}) and a shoulder peak (O_I).

https://doi.org/10.1557/mrc.2014.4 Published online by Cambridge University Press

convert the XPS data to precise values for the oxygen vacancy concentrations, the relative areas beneath the peaks are meaningful. The ratio between the areas under the two peaks, A(O_I)/A(O_{II}), are 0.18 and 0.14 for the VA and OA samples, respectively, and the ratio of the lattice oxygen peaks for each sample, $A(O_{II})_{VA}/A(O_{II})_{OA}$, is 0.96. Thus, the oxygen vacancy concentration increases as the lattice oxygen peak decreases, providing evidence of a non-stochiometric trend due to oxygen vacancy creation from VA. Supplementary materials III(a) provides a comparison of the O 1s peak from the three sample types. Values for A(O_I)/A(O_{II}) and the relative $A(O_{II})/A(O_{II})_{OA}$ ratio are seen in Supplementary materials III(b). These results confirm the generation of oxygen vacancies under VA and the reduction of oxygen vacancies after OA.

Quantitative values of the oxygen vacancy concentration, estimated from the O 1s peak, show a proportional correlation with the extracted BMP density. As the oxygen vacancy concentration increases, the number of trapped electrons and polarons increases, decreasing the electrical resistivity and increasing the carrier concentration. The relative oxygen vacancy concentration is consistent with the changes in M_s, giving direct correlational evidence that the origin of RTFM may be oxygen vacancies.

In summary, the magnetic properties of single-crystal TI candidate SSO thin films have been found to strongly depend on post-growth annealing treatments. VA enhances M_s and H_c, whereas OA degrades both properties. The difference between the effects of VA and OA, supported by the XPS measurements of the oxygen vacancy concentration, indicate that the RTFM is not due to a magnetic impurity but rather related to the oxygen vacancy concentration. Furthermore, the results are explained quantitatively through the BMP model. A linearly proportional correlation is found between the extracted densities of BMP to the XPS O 1s values. These findings provide insight into defect-engineered RTFM of pure SSO and constitute an important step for development of practical spintronic devices.

Supplementary materials

For supplementary material for this article, please visit http://dx.doi.org/10.1557/mrc.2014.4

Acknowledgments

The authors acknowledge the use of the Analytical Instrumentation Facility (AIF) at North Carolina State University, which is supported by the State of North Carolina and the National Science Foundation, and thank Dr. Srinivasa Rao Singamaneni for the stimulating scientific discussion and critical reading of the manuscript.

References

1. B.A. Bernevig and S-C. Zhang: Quantum spin Hall effect. *Phys. Rev. Lett.* **96**, 106802 (2006).
2. J.E. Moore and L. Balents: Topological invariants of time-reversal-invariant band structures. *Phys. Rev. B* **75**, 121306 (2007).
3. L. Fu, C.L. Kane, and E.J. Mele: Topological insulators in three dimensions. *Phys. Rev. Lett.* **98**, 106803 (2007).
4. J-M. Zhang, W. Zhu, Y. Zhang, D. Xiao, and Y. Yao: Tailoring magnetic doping in the topological insulator Bi_2Se_3. *Phys. Rev. Lett.* **109**, 266405 (2012).
5. J. Li, Y. Jiang, Y. Li, D. Yang, Y. Xu, and M. Yan: Origin of room temperature ferromagnetism in MgO films. *Appl. Phys. Lett.* **102**, 072406-(2013).
6. Q. Liu, C-X. Liu, C. Xu, X-L. Qi, and S-C. Zhang: Magnetic impurities on the surface of a topological insulator. *Phys. Rev. Lett.* **102**, 156603 (2009).
7. M. Liu, J. Zhang, C-Z. Chang, Z. Zhang, X. Feng, K. Li, K. He, L-l. Wang, X. Chen, X. Dai, Z. Fang, Q-K. Xue, X. Ma, and Y. Wang: Crossover between weak antilocalization and weak localization in a magnetically doped topological insulator. *Phys. Rev. Lett.* **108**, 036805 (2012).
8. Y.L. Chen, J-H. Chu, J.G. Analytis, Z.K. Liu, K. Igarashi, H-H. Kuo, X.L. Qi, S.K. Mo, R.G. Moore, D.H. Lu, M. Hashimoto, T. Sasagawa, S.C. Zhang, I. R. Fisher, Z. Hussain, and Z.X. Shen: Massive Dirac Fermion on the surface of a magnetically doped topological insulator. *Science* **329**, 659–662 (2010).
9. X-L. Qi, R. Li, J. Zang, and S-C. Zhang: Inducing a magnetic monopole with topological surface states. *Science* **323**, 1184–1187 (2009).
10. H. Pan, J.B. Yi, L. Shen, R.Q. Wu, J.H. Yang, J.Y. Lin, Y.P. Feng, J. Ding, L.H. Van, and J.H. Yin: Room-temperature ferromagnetism in carbon-doped ZnO. *Phys. Rev. Lett.* **99**, 127201 (2007).
11. M. Venkatesan, C.B. Fitzgerald, and J.M.D. Coey: Unexpected magnetism in a dielectric oxide. *Nature* **430**, 630–630 (2004).
12. S. Zhou, E. Čižmár, K. Potzger, M. Krause, G. Talut, M. Helm, J. Fassbender, S.A. Zvyagin, J. Wosnitza, and H. Schmidt: Origin of magnetic moments in defective TiO_2 single crystals. *Phys. Rev. B* **79**, 113201 (2009).
13. S.D. Yoon, Y. Chen, A. Yang, T.L. Goodrich, X. Zuo, D.A. Arena, K. Ziemer, C. Vittoria, and V.G. Harris: Oxygen-defect-induced magnetism to 880 K in semiconducting anatase $TiO_{2-\delta}$ films. *J. Phys.: Condens. Matter* **18**, L355 (2006).
14. C. Sudakar, P. Kharel, R. Suryanarayanan, J.S. Thakur, V.M. Naik, R. Naik, and G. Lawes: Room temperature ferromagnetism in vacuum-annealed TiO2 thin films. *J. Magn. Magn. Mater.* **320**, L31–L36 (2008).
15. H. Ohno: Making nonmagnetic semiconductors ferromagnetic. *Science* **281**, 951–956 (1998).
16. D. Kim, J. Hong, Y.R. Park, and K.J. Kim: The origin of oxygen vacancy induced ferromagnetism in undoped TiO_2. *J. Phys.: Condens. Matter* **21**, 195405 (2009).
17. S. Mal, T-H. Yang, P. Gupta, J.T. Prater, and J. Narayan: Thin film epitaxy and magnetic properties of STO/TiN buffered ZnO on Si(001) substrates. *Acta Mater.* **59**, 2526–2534 (2011).
18. M. Klintenberg: The search for strong topological insulators. *Preprint 2010 arXiv1007.4838K*, 2010.
19. A. Widera and H. Schäfer: Übergangsformen zwischen zintlphasen und echten salzen: Die verbindungen A3BO (MIT A = Ca, Sr, Ba und B = Sn, Pb). *Mater. Res. Bull.* **15**, 1805–1809 (1980).
20. Y.F. Lee, F. Wu, R. Kumar, F. Hunte, J. Schwartz, and J. Narayan: Epitaxial integration of dilute magnetic semiconductor Sr3SnO with Si (001). *Appl. Phys. Lett.* **103**, 112101 (2013).
21. M.W. Thompson: *Defects and Radiation Damage in Metals* (London, Cambridge University Press, vol. Chap. 2, 1969), p. 11.
22. S. Banerjee, M. Mandal, N. Gayathri, and M. Sardar: Enhancement of ferromagnetism upon thermal annealing in pure ZnO. *Appl. Phys. Lett.* **91**, 182501 (2007).
23. J.M.D. Coey: Dilute magnetic oxides. *Curr. Opin. Solid State Mater. Sci.* **10**, 83–92 (2006).
24. J.E. Jaffe, T.C. Droubay, and S.A. Chambers: Oxygen vacancies and ferromagnetism in $Co_xTi_{1-x}O_{2-x-y}$. *J. Appl. Phys.* **97**, 073908 (2005).
25. J.M.D. Coey, K. Wongsaprom, J. Alaria, and M. Venkatesan: Charge-transfer ferromagnetism in oxide nanoparticles. *J. Phys. D: Appl. Phys.* **41**, 134012 (2008).
26. A.F. Kohan, G. Ceder, D. Morgan, and C.G. Van de Walle: First-principles study of native point defects in ZnO. *Phys. Rev. B* **61**, 15019 (2000).

https://doi.org/10.1557/mrc.2014.4 Published online by Cambridge University Press

27. C. Chiorescu, J.L. Cohn, and J.J. Neumeier: Impurity conduction and magnetic polarons in antiferromagnetic oxides. *Phys. Rev. B* **76**, 020404 (2007).
28. J.M.D. Coey, M. Venkatesan, and C.B. Fitzgerald: Donor impurity band exchange in dilute ferromagnetic oxides. *Nat. Mater.* **4**, 173 (2005).
29. W.R.C. Wagner, L. Davis, and J. Moulder: *Handbook of X-ray Photoelectron Spectroscopy* (PerkinElmer Corporation, Eden Prairie, Minnesota, 1979).
30. T.J. Chuang, C.R. Brundle, and D.W. Rice: Interpretation of the x-ray photoemission spectra of cobalt oxides and cobalt oxide surfaces. *Surface Sci.* **59**, 413 (1976).

https://doi.org/10.1557/mrc.2014.4 Published online by Cambridge University Press